Thin Solid Films 556 (2014) 503–508

Contents lists available at ScienceDirect

Thin Solid Films

journal homepage: www.elsevier.com/locate/tsf

Ultrathin SnO_2 layer for efficient carrier collection in dye-sensitized solar cells

Seok-Min Yong, Nikolay Tsvetkov, Liudmila Larina, Byung Tae Ahn, Do Kyung Kim [1]

Department of Materials Science and Engineering, Korea Advanced Institute of Science and Technology (KAIST), 335 Gwahangno, Yuseong-gu, Daejeon 305-701, Republic of Korea

ARTICLE INFO

Article history:
Received 15 June 2013
Received in revised form 3 January 2014
Accepted 3 January 2014
Available online 9 January 2014

Keywords:
Dye-sensitized solar cells
Recombination
Tin dioxide
Blocking layer
Tin chloride treatment

ABSTRACT

An ultrathin SnO_2 layer was introduced as a blocking layer in dye-sensitized solar cells (DSSCs) for improving conversion efficiency. The SnO_2 blocking layer, composed of approximately 10 nm nanoparticles, was deposited on the fluorine-doped tin oxide (FTO) coated glass by $SnCl_4$ treatment, a simple and inexpensive method. This SnO_2 blocking layer increased the onset of dark current from FTO to electrolyte, suppressing charge recombination at the FTO/electrolyte interface. The cascading band structure of TiO_2 and SnO_2 increased the charge carrier lifetime, resulting in effective charge collection. Examining DSSC performance as a function of $SnCl_4$ treatment time, a peak conversion efficiency of 7.33% was achieved for a $SnCl_4$ treatment time of 15 min (SnO_2 layer thickness ~ 12 nm), compared to 6.08% for an untreated cell. Also, compared to a TiO_2 blocking layer, the SnO_2 blocking layer showed a higher performance.

1. Introduction

Since O'Regan and Grätzel reported the first dye-sensitized solar cells (DSSCs) in 1991 [1], they have attracted considerable attention as potential replacements for conventional Si-based solar cells in specialized applications due to their low production cost, easy fabrication, lightweight, and flexibility [2–4]. Generally, a DSSC has a sandwich type structure, composed of fluorine-doped tin oxide coated glass (FTO glass), a TiO_2 mesoporous layer (photoelectrode), dye molecules adsorbed on the TiO_2 surface, a redox electrolyte (iodide/tri-iodide couple), and Pt-coated FTO glass (counter electrode). When a photon is absorbed by a dye molecule, the excited dye transfers an electron to the conduction band of a TiO_2 nanoparticle. The oxidized dye is reduced by iodide in the electrolyte. The photo-injected electron in the TiO_2 photoelectrode passes through the external load and reduces tri-iodide to iodide at the counter electrode [5].

Thus far, cell and submodule overall conversion efficiencies have reached 11.9% and 9.9%, respectively [6]. Despite drastic efficiency improvements in DSSCs, they are still too insufficient for industrial applications. Therefore, improving conversion efficiency is a major issue for DSSCs.

In DSSCs, FTO glass can directly contact the electrolyte because the mesoporous TiO_2 photoelectrode cannot uniformly cover the entire FTO surface. At the FTO/electrolyte interface, charge recombination occurs, which is one of the limiting factors of electron collection in DSSCs [7–11]. Thus, modifying the FTO/electrolyte interface to suppress the recombination reaction from FTO to electrolyte is important to improve the DSSC performance. One promising approach is to add a compact metal oxide blocking layer to the FTO glass that would impede back electron transport from the FTO glass to the electrolyte [12]. In the past decade, the effectiveness of various metal oxides as a blocking layer has been demonstrated. Ito et al. [12,13] and Choi et al. [14] demonstrated that a TiO_2 blocking layer prepared via $TiCl_4$ treatment shifts the dark current onset by several hundred millivolts and increases the interfacial charge-transfer resistance between FTO glass and electrolyte. Xia et al. [15] reported that a spray-fabricated Nb_2O_5 blocking layer greatly increases shunt resistance and decreases series resistance. Roh et al. [16] showed that a ZnO blocking layer, developed by a simple chemical method, serves as an inherent energy barrier for avoiding recombination losses.

SnO_2, an n-type semiconductor oxide with a 3.8 eV band gap [17,18], is a promising blocking layer candidate. SnO_2 is transparent, chemically stable, and has high electron mobility (100–200 cm^2/Vs) [19–22]. SnO_2 also creates a cascading band structure when layered with the TiO_2 photoelectrode and N719 dye [23,24]. It has been reported that, based on the electron transfer process in a photosynthetic system, multistep electron transport down a cascading band structure increases carrier lifetime and reduces charge recombination [25,26]. Ravirajan et al. [27] and Spoerke et al. [25] reported that formation of a cascading band structure by modifying the poly-3-hexylthiophene (P3HT)/ZnO interface of a P3HT/ZnO hybrid solar cell with a ruthenium dye and nanocrystalline CdS enhanced carrier lifetimes and conversion efficiency.

There have been only two reports on the introduction of SnO_2 blocking layer between the TiO_2 photoelectrode and FTO glass to improve DSSC performance. Kim et al. [9] and Duong et al. [28] employed the SnO_2 blocking layer using layer-by-layer deposition of SnO_2 nanoparticles and nanocluster deposition method, respectively,

E-mail address: dkkim@kaist.ac.kr (D.K. Kim).
[1] Tel.: +82 42 350 4118; fax: +82 42 350 3310.

0040-6090/$ – see front matter
http://dx.doi.org/10.1016/j.tsf.2014.01.008

resulting in the improvement of conversion efficiencies. However, these methods have some drawbacks such as complexity and high manufacturing cost. In the present work, we present a simple and inexpensive method, $SnCl_4$ treatment, to deposit an ultrathin SnO_2 blocking layer on the FTO glass. It was found that introduction of the ultrathin SnO_2 blocking layer effectively increased photovoltaic performance of DSSC. The deposition mechanism and influence of $SnCl_4$ treatment time on DSSC performance were also investigated.

2. Experimental section

Anatase TiO_2 nanoparticles for the photoelectrode were synthesized following an experimental procedure previously reported by our group [29]. The prepared TiO_2 nanoparticles were diamond shaped and approximately 25 nm across.

Details of the electrode fabrication and DSSC assembly have been described elsewhere [13]. The FTO glass (7 Ω/cm^2) was sequentially cleaned in acetone, 0.1 M HCl ethanolic solution, deionized water, and ethanol. After cleaning, it was treated with a 40 mM $SnCl_4$ aqueous solution at 70 °C for various times (5, 15, 30, 60, and 90 min) to deposit a compact SnO_2 blocking layer. Then, the FTO glass was coated in TiO_2 paste using the doctor-blade method. The paste was prepared by mixing anatase TiO_2 nanoparticles with terpineol and ethyl cellulose ethanol solution. This mixture was then sonicated and stirred for 24 h. Ethanol was removed from the solution with a rotary evaporator. The final paste contained 18 wt.% TiO_2, 9 wt.% ethyl cellulose, and 73 wt.% terpineol. Finally, the TiO_2 film was sintered in air at 500 °C for 15 min. The photoelectrode film thickness was measured to be approximately 8.5 μm.

For the dye coating, the photoelectrodes were dipped in a 0.5 mM N719 dye solution in a mixture of acetonitrile and *tert*-butyl alcohol (1:1 volume ratio) for 24 h. After sensitizer uptake, the photoelectrodes were washed with acetonitile. Platinum-coated FTO glass was used as a counter electrode. The platinum coating was produced by thermal

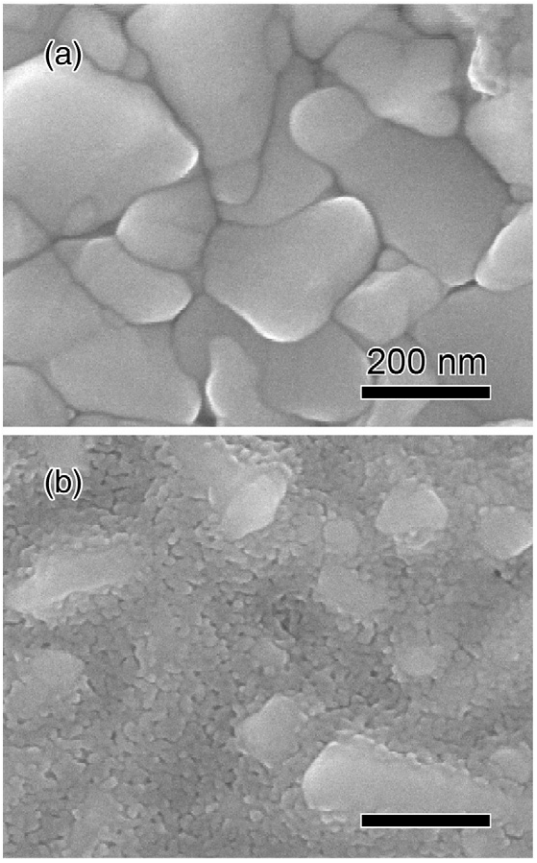

Fig. 1. SEM micrographs showing the top surface of (a) FTO glass and (b) BL-15/FTO.

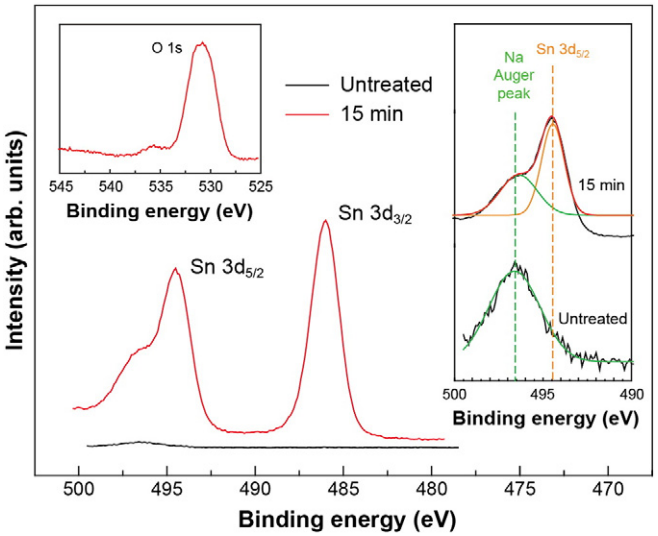

Fig. 2. Sn 3d transition peaks in XPS spectra of bare SLG and BL-15/SLG. Left and right insets show the O 1s transition peak for BL-15/SLG and deconvolution result of the Sn $3d_{5/2}$ peak.

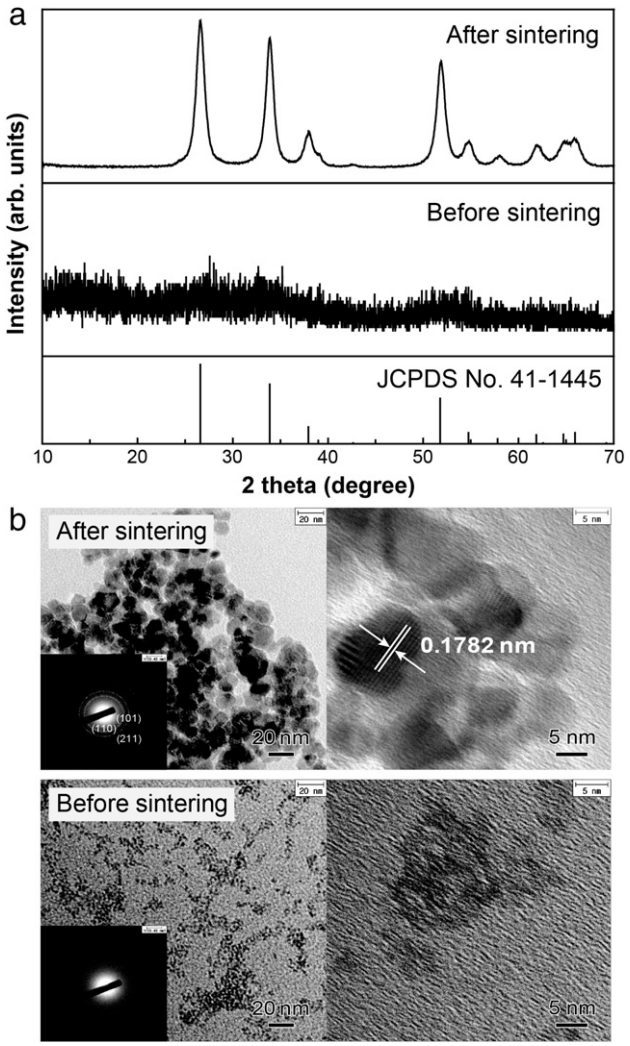

Fig. 3. (a) XRD patterns and (b) TEM micrographs of the white precipitate, formed during $SnCl_4$ treatment, before and after sintering at 500 °C for 15 min.

Table 1
Photovoltaic properties of cells fabricated with SnO_2 and TiO_2 blocking layers.

DSSC	SnO_2 blocking layer thickness [nm]	J_{SC} [mA/cm^2]	V_{OC} [V]	FF	η [%]
C-BL-0	0	12.15 ± 0.34	0.724 ± 0.016	69.18 ± 2.97	6.08 ± 0.33
C-BL-5	9.92 ± 1.80	12.59 ± 0.55	0.732 ± 0.034	69.03 ± 2.21	6.35 ± 0.27
C-BL-15	11.72 ± 2.76	13.66 ± 0.75	0.744 ± 0.009	72.12 ± 0.90	7.33 ± 0.29
C-BL-30	13.44 ± 5.66	13.02 ± 1.63	0.721 ± 0.037	68.68 ± 4.57	6.41 ± 0.44
C-BL-60	18.76 ± 6.86	12.68 ± 0.92	0.662 ± 0.030	63.07 ± 1.74	5.28 ± 0.23
C-BL-90	25.67 ± 14.24	12.98 ± 0.18	0.634 ± 0.024	59.93 ± 2.64	4.93 ± 0.34
Cell based on TiO_2 blocking layer		12.37 ± 1.18	0.777 ± 0.025	73.93 ± 1.26	7.07 ± 0.39

The data presented are the average of five cells.

decomposition of H_2PtCl_6. The counter- and photoelectrodes were assembled into a sandwich-type cell and sealed with an ionomer film (Meltonix 1170–60). The internal cell space was filled with commercially available liquid electrolyte, AN-50 (Solaronix), by capillary action. The active area of the fabricated cells varied from 0.14 to 0.16 cm^2. In this paper, BL-x denotes the blocking layer formed by $SnCl_4$ treatment for *x* minutes. The cell fabricated including BL x is denoted C-BL-x.

The surface morphology of the blocking layer was observed via scanning electron microscopy (SEM, XL30, Philips, Netherlands) under operating voltage of 10 kV. Its chemical composition was investigated via X-ray photoelectron spectroscopy (XPS), using a Sigma Probe (VG Scientific) with Al Ka (1486.65 eV) X-ray radiation under a base pressure of 1.33×10^{-8} Pa. The analysis area was 400 μm. The carbon 1s line has been used to calibrate the binding energy scale for the XPS measurements. The phase of the synthesized product was characterized by an X-ray diffractometer (XRD, D/MAX-IIIC, Rigaku, Japan) with Cu Kα radiation (λ = 0.15406 nm at 40 kV and 45 mA). The thickness of the photoelectrode film was measured with an Alpha Step (Tencor, USA) surface profiler. The transmittance of the SnO_2 layer was measured with a UV/Vis spectrometer (UV-3101PC, Shimadzu Co., Japan). The thickness of the SnO_2 blocking layer was estimated with an elipsometer (α-SE, J. A. Woollam Co., Inc., USA). Room-temperature photoluminescence (PL) spectra were recorded using a fluorescence spectrophotometer (RF-5301PC, Shimadzu Co., Japan).

The current density–voltage (*J*–*V*) characteristics of the fabricated cells were measured under the illumination of a Polaronix K202 (McScience, Korea) equipped with a 100 W Xenon lamp and AM 1.5G filter set. The incident light intensity was set at 100 mW/cm^2 using a PVM-580 Si reference photodiode (PV Measurements Inc., USA). *J*–*V* curves were recorded by applying an external bias to the solar cell and measuring the photocurrent with a photovoltaic power meter (PolaronixK101/LAB20, McScience, Korea).

3. Results and discussion

Fig. 1 shows SEM images of the top surface of bare FTO glass and BL-15/FTO. A difference between bare FTO and BL-15/FTO was clearly observed. After $SnCl_4$ treatment, the nanoparticles with size of 10 nm covered the entire FTO surface, thereby forming a compact layer.

XPS was conducted to investigate the elemental composition of the layer deposited during $SnCl_4$ treatment. Fig. 2 presents a comparison of the Sn 3d transition peaks of bare soda-lime glass (SLG) and BL-15/SLG. In XPS study, the SLG substrate which does not contain Sn was used to avoid the effect of the FTO substrate. Binding energies of 497.6 and 488.3 eV, corresponding to Sn $3d_{5/2}$ and $3d_{3/2}$ peaks, were observed in the $SnCl_4$-treated sample, but no Sn-related peaks were seen in bare SLG. The left-hand inset in Fig. 2 shows the O 1s transition peak (531.0 eV) for BL-15/SLG. These results suggest that a SnO_2 layer was deposited by the $SnCl_4$-treatment. The shoulder beside the Sn $3d_{5/2}$ peak is from a 497 eV, also detected in the untreated sample, as shown by deconvolution in the right-hand inset in Fig. 2. This shoulder peak is likely a Na $KL_{23}L_{23}$ Auger peak from the SLG substrate [30].

We conducted additional experiments to investigate the elemental composition and deposition mechanism of the $SnCl_4$-created layer. During $SnCl_4$ treatment, white particles precipitated out of the $SnCl_4$ aqueous solution. This precipitate was collected and its phase and morphology were analyzed before and after sintering at 500 °C for 15 min. Fig. 3(a) and (b) show XRD patterns and TEM micrographs of the precipitate before and after sintering. The as-collected precipitate is shown to consist of amorphous nanoparticles with size of approximately 3 nm. After sintering, it was confirmed that the amorphous phase changed to SnO_2 (cassiterite, JCPDS No. 41–1445) and the particle size increased to approximately 10 nm, which is consistent with the size observed in Fig. 1. According to these results and the XPS data discussed previously, it is clear that a compact nanocrystalline SnO_2 layer was deposited by the $SnCl_4$ treatment.

Based on above results, a deposition mechanism for the SnO_2 layer via the $SnCl_4$ treatment can be proposed. This deposition process involves three stages: (1) amorphous SnO_2 nuclei are generated across the entire FTO surface, which acts as a nucleation site; (2) crystallization and grain growth of the amorphous SnO_2 nuclei occurs simultaneously during sintering; and (3) a SnO_2 blocking layer composed of nanoparticles (~10 nm) is deposited on the FTO glass.

SnO_2 layer thickness as a function of $SnCl_4$ treatment time is shown in Table 1. The thickness was measured at 10 different locations per sample. For BL-5, the SnO_2 layer is approximately 10 nm thick, similar to the SnO_2 nanoparticle size observed in Fig. 1. These data, supported by the low standard deviation in these measurements, indicate formation of a SnO_2 nanoparticle monolayer at the initial treatment stage. SnO_2 layer thickness increases linearly with treatment time; a thickness of approximately 26 nm is obtained for BL-90. The standard deviation gradually increases as well, indicating increased surface roughness.

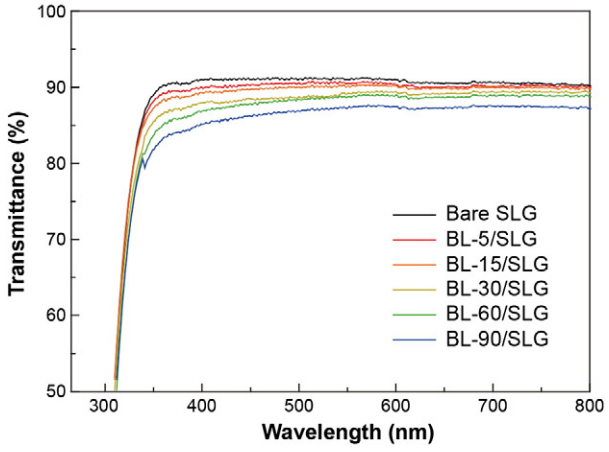

Fig. 4. Optical transmittance spectra of SnO_2/SLGs created with different $SnCl_4$ treatment times.

This might be due to nonhomogeneous nucleation after formation of the nanocrystalline SnO_2 monolayer.

Fig. 4 depicts optical transmittance spectra of SnO_2/SLGs with different $SnCl_4$ treatment times. The transmittance gradually decreases as $SnCl_4$ treatment time increases. It is a small decrease; in the 350–800 nm wavelength range, BL-90/SLG has a transmittance of 87%, whereas bare SLG has a transmittance of 90%. It is inferred that this decrease is caused by the increased SnO_2 layer thickness [31].

To determine the effectiveness of a SnO_2 blocking layer in suppressing recombination at the FTO/electrolyte interface, we fabricated modified cells and measured their dark *J–V* characteristics. The modified cells consisted solely of FTO glass, a SnO_2 blocking layer, electrolyte, Pt, and FTO, but not TiO_2 photoelectrode or dye because we were only interested in the dark current from the FTO glass to electrolyte [13]. Fig. 5(a) and (b) show the dark *J–V* characteristics of the modified cells and the onset of dark current emanating from the SnO_2/FTO glass as a function of $SnCl_4$ treatment time, respectively. The dark current onset was determined by extrapolating the linear region of the dark *J–V* curve to zero. Each data was the average of three modified cells. As shown in Fig. 5(b), the dark current onset of the modified cell employing BL-15/FTO glass was approximately 120 mV higher than that of the modified cell employing bare FTO glass (0.94 → 1.06 V). Thus, the barrier to dark current flow from FTO to electrolyte increased when the SnO_2 layer was included, clearly demonstrating its effectiveness in suppressing charge recombination between the FTO and electrolyte.

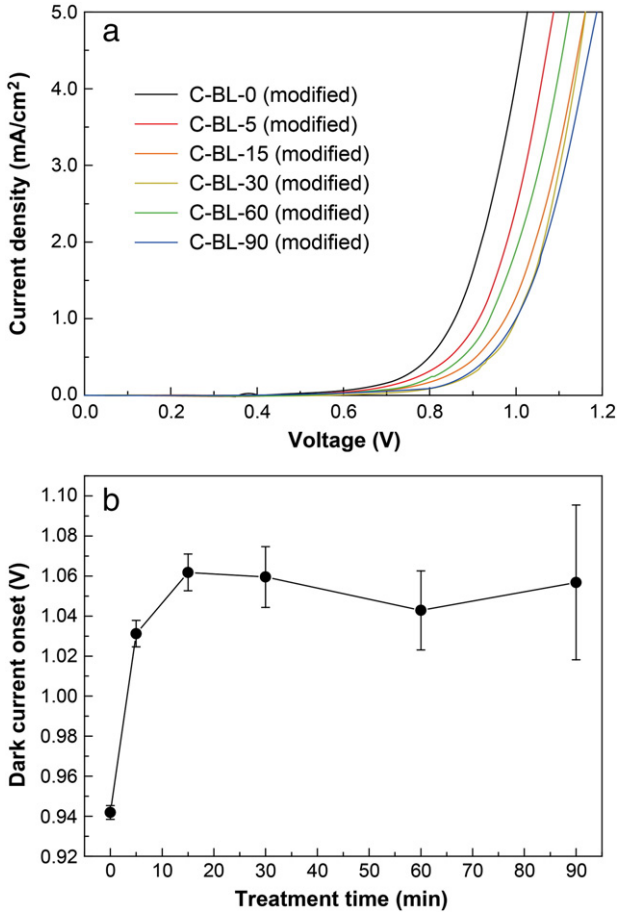

Fig. 5. (a) Dark *J–V* curves of modified cells as a function of $SnCl_4$ treatment time. The modified cells consisted solely of FTO glass, a SnO_2 blocking layer, electrolyte, Pt, and FTO glass. (b) Onset of dark current calculated from dark *J–V* curve as a function of $SnCl_4$ treatment time. Dark current onset was determined by extrapolating the linear region of the dark J–V curve to zero. Each data was the average of three modified cells.

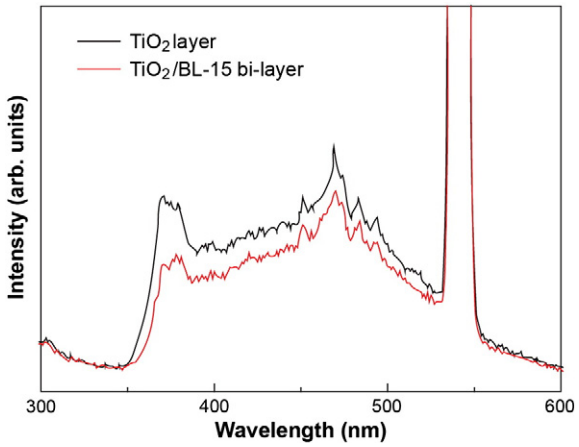

Fig. 6. PL spectra of the TiO_2 layer and TiO_2/BL-15 bi-layer.

Fig. 6 shows PL spectra for the TiO_2 layer and TiO_2/BL-15 bi-layer (excitation at 270 nm). The PL spectra are characterized by two peaks at approximately 374 and 470 nm, which correspond to the band-gap transition and surface oxygen vacancies, respectively [32]. The intense peak at 540 nm originates from scattering and diffraction of the 270 nm excitation beam. The PL intensity of the TiO_2/BL-15 bi-layer was lower than that of the TiO_2 layer, indicating reduced charge recombination. This PL quenching might be induced by the cascading band structure of TiO_2 and SnO_2 [33–35]. The bottom of the conduction band and top of the valence band of TiO_2 were both higher than those of SnO_2. Thus, photo-generated electrons in TiO_2 can migrate easily into SnO_2, decreasing the recombination rate of photo-generated electrons (Scheme 1). Therefore, introduction of a SnO_2 blocking layer can increase charge carrier lifetimes and improve the collection efficiency of photo-injected electrons in DSSCs.

Fig. 7 shows the *J–V* curve of the fabricated cells employing bare FTO and SnO_2/FTO. The photovoltaic properties of the fabricated cells employing bare FTO and SnO_2/FTO as a function of $SnCl_4$ treatment time are shown in Fig. 8 and summarized in Table 1. Each data was the average of five cells. Fig. 8(a) presents the open-circuit voltage (V_{OC}) as a function of $SnCl_4$ treatment time. C-BL-0 exhibits a V_{OC} of approximately 0.724 V, which agrees well with values reported in other papers [14,36,37]. The V_{OC} increased slowly, peaking at 0.744 V for a treatment time of 15 min before gradually decreasing. Introduction of a SnO_2 blocking layer could affect the V_{OC} both positively and negatively. The V_{OC} could be improved by suppression of the recombination reaction. V_{OC} is determined by the difference between Fermi level of

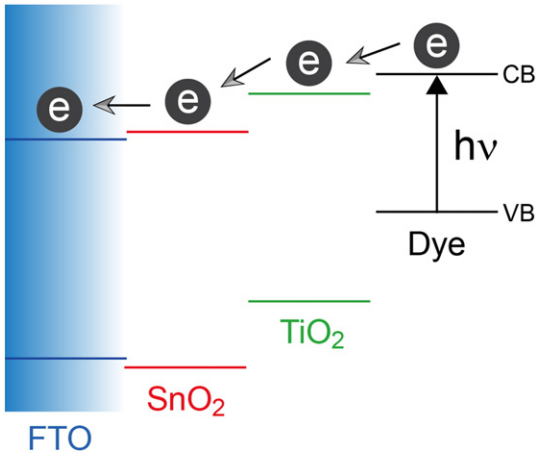

Scheme 1. Schematic for cascading band structure formed by introducing SnO_2 blocking layer between FTO glass and TiO_2 photoelectrode.

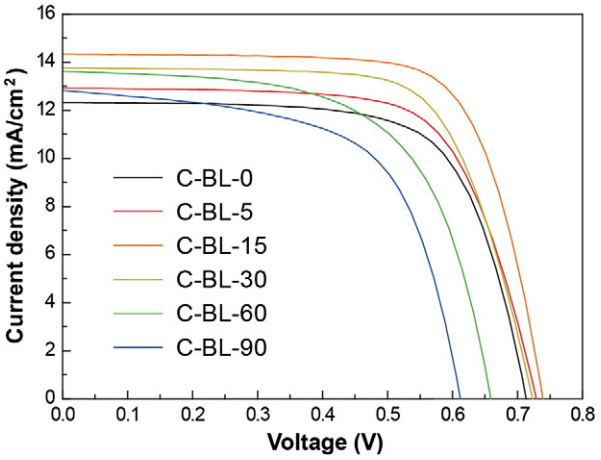

Fig. 7. *J–V* curves of the fabricated cells employing bare FTO and SnO_2/FTO.

the photoelectrode and redox potential of electrolyte [2]. As shown in Fig. 6, the SnO_2 blocking layer effectively prohibits recombination at the FTO/electrolyte interface. Reduced recombination shifts the Fermi level upward by increasing the electron concentration, leading to a potential increase in V_{OC} [38]. On the other hand, because the conduction band edge of SnO_2 (approximately 0.5 eV) is lower than that of anatase TiO_2 [17], the Fermi level of the photoelectrode could be shifted down, decreasing V_{OC} [24]. Based on the data collected, up to a treatment time 15 min, the first effect is more prominent, producing an improved V_{OC}. After 15 min, the second effect dominates due to the increased layer thickness, decreasing the V_{OC}.

The short-circuit current density (J_{SC}) and fill factor (FF) as a function of $SnCl_4$ treatment time are displayed in Fig. 8(b) and (c), respectively. These parameters exhibit trends similar to V_{OC}. Despite the slight decrease in transmittance shown in Fig. 4, C-BL-15 achieved the highest J_{SC} (13.66 mA/cm^2) and FF (72.12), compared to those of C-BL-0, 12.15 mA/cm^2 and 69.18, respectively. Several factors may have contributed to these J_{SC} and FF improvements: (1) the SnO_2 blocking layer prevents unidirectional charge flow from the FTO to the electrolyte, (2) carrier lifetime increases due to multistep electron transport down the cascading band structure (dye/TiO_2/SnO_2), and (3) the bond strength between the FTO and TiO_2 photoelectrode is enhanced by the compact SnO_2 layer [13], helping collection of photo-injected electrons. However, for treatment times longer than 15 min, J_{SC} and FF decreased. This might have been caused by the increased SnO_2 layer thickness and surface roughness. Thicker, rougher layers provide more trap sites, obstructing collection of photo-injected electrons [14].

Fig. 8(d) shows the conversion efficiency (η) of the fabricated cells employing bare FTO and SnO_2/FTO as a function of treatment time. C-BL-15 showed the highest efficiency of 7.33%, compared to 6.08% for C-BL-0. This rate of increase is similar with the reported papers related to the SnO_2 blocking layer [9,28]. Based on the V_{OC}, J_{SC} and FF results, this enhancement can be attributed mainly to the suppression of recombination at the FTO/electrolyte interface by the SnO_2 blocking layer and the increased carrier lifetime provided by multistep electron transport down a cascading band structure (dye/TiO_2/SnO_2).

The performance of the cell based on the SnO_2 blocking layer (C-BL-15) was compared to that of the cell based on TiO_2 blocking layer. The TiO_2 blocking layer was deposited on the FTO glass through a $TiCl_4$ treatment (40 mM $TiCl_4$ aqueous solution, 70 °C, and 30 min), which is the common approach in the DSSCs [12,13,39]. As shown in Table 1, the cell based on the TiO_2 blocking layer showed J_{SC} = 12.37 mA/cm^2, V_{OC} = 0.777 V, FF = 73.93, and η = 7.07%. The J_{SC} value of C-BL-15 is higher than that of the cell based on TiO_2 blocking layer. This is predominantly contributed to the increased carrier lifetime by the formation of a cascading band structure (dye/TiO_2/SnO_2). On the other hand, the V_{OC} value of C-BL-15 is lower than that of the cell based on the TiO_2 blocking layer. This is caused by the lower conduction band edge of SnO_2 than

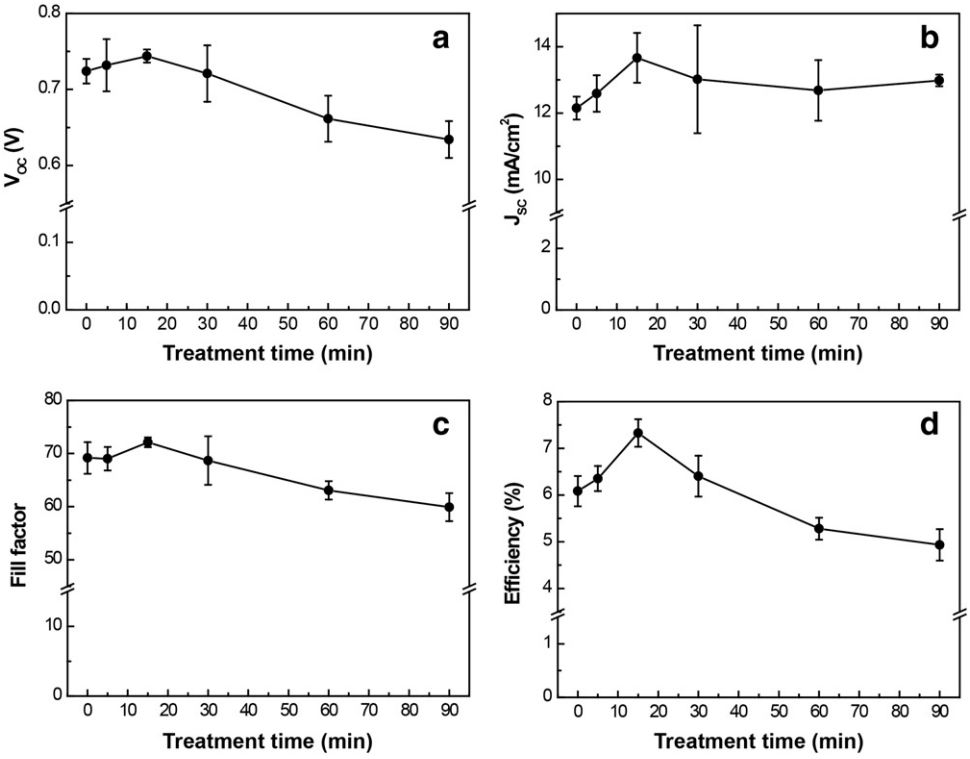

Fig. 8. (a) Open-circuit voltage, (b) short-circuit current density, (c) fill factor, and (d) conversion efficiency of the fabricated cells employing bare FTO and SnO_2/FTO as a function of $SnCl_4$ treatment time. Each data was the average of five cells.

TiO_2. Consequently, C-BL-15 showed the slightly higher conversion efficiency than the cell based on TiO_2 blocking layer. It is expected that the conversion efficiency of the cell based on SnO_2 blocking layer can be enhanced by improving the V_{OC} through the modification of the band structure of the SnO_2 layer.

4. Conclusion

In summary, SnO_2 was introduced as a blocking layer material in DSSCs. An ultrathin, transparent SnO_2 blocking layer, composed of approximately 10 nm nanoparticles, was deposited via $SnCl_4$ treatment which is a simple method. The SnO_2 layer thickness increased from 10 to 26 nm when treatment time increased from 5 to 90 min. A maximum conversion efficiency of 7.33% was obtained at a $SnCl_4$ treatment time of 15 min (SnO_2 layer thickness ~12 nm), compared to 6.08% for an untreated cell. This performance improvement was attributed to the suppression of charge recombination at the FTO/electrolyte interface and increased carrier lifetime provided by multistep electron transport down the cascading band structure (dye/TiO_2/SnO_2), both of which improved charge collection. Compared to the cell based on TiO_2 blocking layer, the cell based on SnO_2 blocking layer showed the slightly higher conversion efficiency. Our results suggest that introduction of a SnO_2 blocking layer is a promising and effective method for improving the photovoltaic performance of DSSCs.

Acknowledgment

This work was supported by Basic Science Research Program (2009–0094038) and the Pioneer Research Center Program (2010–0019469) through the National Research Foundation of Korea (NRF) funded by the Ministry of Education, Science and Technology.

References

[1] B. Oregan, M. Gratzel, Nature 353 (1991) 737.
[2] A. Hagfeldt, G. Boschloo, L.C. Sun, L. Kloo, H. Pettersson, Chem. Rev. 110 (2010) 6595.
[3] S.M. Yong, T. Nikolay, B.T. Ahn, D.K. Kim, J. Alloy. Compd. 547 (2013) 113.
[4] R.H. Lee, Y.W. Huang, Thin Solid Films 517 (2009) 5903.
[5] Y.H. Luo, D.M. Li, Q.B. Meng, Adv. Mater. 21 (2009) 4647.
[6] M.A. Green, K. Emery, Y. Hishikawa, W. Warta, E.D. Dunlop, Prog. Photovoltaics 21 (2013) 1.
[7] K. Zhu, E.A. Schiff, N.G. Park, J. van de Lagemaat, A.J. Frank, Appl. Phys. Lett. 80 (2002) 685.
[8] F. Fabregat-Santiago, J. Bisquert, G. Garcia-Belmonte, G. Boschloo, A. Hagfeldt, Sol. Energy Mater. Sol. C 87 (2005) 117.
[9] Y.J. Kim, K.H. Kim, P. Kong, H.J. Kim, Y.S. Choi, W.I. Lee, Langmuir 28 (2012) 10620.
[10] Q. Wang, S. Ito, M. Gratzel, F. Fabregat-Santiago, I. Mora-Sero, J. Bisquert, T. Bessho, H. Imai, J. Phys. Chem. B 110 (2006) 25210.
[11] F. Fabregat-Santiago, G. Garcia-Belmonte, I. Mora-Sero, J. Bisquert, Phys. Chem. Chem. Phys. 13 (2011) 9083.
[12] S. Ito, P. Liska, P. Comte, R.L. Charvet, P. Pechy, U. Bach, L. Schmidt-Mende, S.M. Zakeeruddin, A. Kay, M.K. Nazeeruddin, M. Gratzel, Chem. Commun. (2005) 4351.
[13] S. Ito, T.N. Murakami, P. Comte, P. Liska, C. Gratzel, M.K. Nazeeruddin, M. Gratzel, Thin Solid Films 516 (2008) 4613.
[14] H. Choi, C. Nahm, J. Kim, J. Moon, S. Nam, D.R. Jung, B. Park, Curr. Appl. Phys. 12 (2012) 737.
[15] J.B. Xia, N. Masaki, K.J. Jiang, S. Yanagida, J. Photochem. Photobiol. A 188 (2007) 120.
[16] S.J. Roh, R.S. Mane, S.K. Min, W.J. Lee, C.D. Lokhande, S.H. Han, Appl. Phys. Lett. 89 (2006) 253512.
[17] M. Gratzel, Nature 414 (2001) 338.
[18] R.Y. Korotkov, P. Ricou, A.J.E. Farran, Thin Solid Films 502 (2006) 79.
[19] E. Ramasamy, J. Lee, Energy Environ. Sci. 4 (2011) 2529.
[20] X.C. Dou, D. Sabba, N. Mathews, L.H. Wong, Y.M. Lam, S. Mhaisalkar, Chem. Mater. 23 (2011) 3938.
[21] M. Okuya, S. Kaneko, K. Hiroshima, I. Yagi, K. Murakami, J. Eur. Ceram. Soc. 21 (2001) 2099.
[22] X.C. Dou, R.R. Prabhakar, N. Mathews, Y.M. Lam, S. Mhaisalkar, J. Electrochem. Soc. 159 (2012) H735.
[23] H.J. Snaith, C. Ducati, Nano Lett. 10 (2010) 1259.
[24] Z.Y. Liu, K. Pan, Q.L. Zhang, M. Liu, R.K. Jia, Q. Lu, D.J. Wang, Y.B. Bai, T.J. Li, Thin Solid Films 468 (2004) 291.
[25] E.D. Spoerke, M.T. Lloyd, E.M. McCready, D.C. Olson, Y.J. Lee, J.W.P. Hsu, Appl. Phys. Lett. 95 (2009).
[26] D. Gust, T.A. Moore, A.L. Moore, Acc. Chem. Res. 34 (2001) 40.
[27] P. Ravirajan, A.M. Peiro, M.K. Nazeeruddin, M. Graetzel, D.D.C. Bradley, J.R. Durrant, J. Nelson, J. Phys. Chem. B 110 (2006) 7635.
[28] T.T. Duong, H.J. Choi, Q.J. He, A.T. Le, S.G. Yoon, J. Alloy. Compd. 561 (2013) 206.
[29] C.H. Cho, M.H. Han, D.H. Kim, D.K. Kim, Mater. Chem. Phys. 92 (2005) 104.
[30] Q.H. Wu, A. Thissen, W. Jaegermann, Appl. Surf. Sci. 252 (2005) 1801.
[31] T.R. Giraldi, M.T. Escote, M.I.B. Bernardi, V. Bouquet, E.R. Leite, E. Longo, J.A. Varela, J. Electroceram. 13 (2004) 159.
[32] B. Chai, T.Y. Peng, X.H. Zhang, J. Mao, K. Li, X.G. Zhang, Dalton Trans. 42 (2013) 3402.
[33] K. Vinodgopal, P.V. Kamat, Environ. Sci. Technol. 29 (1995) 841.
[34] Z.Y. Liu, D.D.L. Sun, P. Guo, J.O. Leckie, Nano Lett. 7 (2007) 1081.
[35] S.H. Hwang, C. Kim, J. Jang, Catal. Commun. 12 (2011) 1037.
[36] F. Sauvage, F. Di Fonzo, A.L. Bassi, C.S. Casari, V. Russo, G. Divitini, C. Ducati, C.E. Bottani, P. Comte, M. Graetzel, Nano Lett. 10 (2010) 2562.
[37] T.L. Ma, M. Akiyama, E. Abe, I. Imai, Nano Lett. 5 (2005) 2543.
[38] J.S. Im, S.K. Lee, Y.S. Lee, Appl. Surf. Sci. 257 (2011) 2164.
[39] T. Nikolay, L. Larina, O. Shevaleevskiy, B.T. Ahn, Energy Environ. Sci. 4 (2011) 1480.